

Optimum design of stiffened plates for static or dynamic loadings using different ribs

Zoltán Virág^{1a} and Károly Jármái²

¹Institute of Mining and Geotechnical Engineering, University of Miskolc H-3515 Miskolc, Egyetemváros, Hungary

²Institute of Energy Engineering and Chemical Machinery, University of Miskolc H-3515 Miskolc, Egyetemváros, Hungary

(Received August 10, 2017, Revised June 5, 2019, Accepted December 15, 2019)

Abstract. The main requirements of modern welded metal structures are the load-carrying capacity (safety), fitness for production, and economy. The primary objective of attaching longitudinal stiffeners is to improve the buckling strength of relatively thin compression panels. This paper gives several comparisons for stiffened plates with different loadings (static, dynamic), different shape of stiffeners (flat, L-shape, trapezoidal), different steel grades, and different welding technologies (SMAW, GMAW, SAW), different costs to show the necessity of a combination of design, fabrication and economic aspects. Safety and fitness for production are guaranteed by fulfilling the design and fabrication constraints. The economy is achieved by minimizing the cost function. It is shown that the optimum sizes depend on the welding technology, the material yield stress, the profile of the stiffeners, the load cycles and the place of the production.

Keywords: stiffened plates; stability; optimum design; static; fatigue loading; cost calculation

1. Introduction

Welded stiffened plates and shells are widely used in various structures, e.g. bridges, ships, bunkers, tank roofs, vehicles, etc. They are subject to multiple loadings: compression, shear, bending or combined load (Bourada 2019). The shape of the plates can be square, rectangular, circular, trapezoidal, etc. Plates and shells can be stiffened in one or two directions with stiffeners of many different shapes.

Various types of loadings and stiffener shapes have been investigated Tran *et al.* (2014), Virág & Jármái (2003). They have investigated mostly the flat, the L-shape, the trapezoidal stiffeners. The optimization of stiffened plates and shells shows the necessity of mass and cost reductions (Jármái *et al.* 2006, Simoes *et al.* 2015, Jin *et al.* 2014, Yoo *et al.* 2014, Mittelstedt C. 2008) considered, but the free vibration can also have an impact on the structural behaviour (Nguyen-Thoi 2013). Stability issues can play also a considerable effect on the sizes of the structures: local, overall and torsional (Kim *et al.* 2018). Stiffeners can have a good effect on local buckling. Kim *et al.* dealt with web plate buckling with stiffeners (Kim *et al.* 2019). Using different materials is investigated by Fernandes and Neto (2015). In some cases, the shear deformation can play an important role (Klouche *et al.* 2017). The combination of steel and fiber reinforced composite is also a way to reduce the mass of the structure (Kovács and Farkas 2017, Remil *et al.* 2019) The static loads are uniaxial compression and

lateral pressure, and the dynamic load is for fatigue. The structural optimization of different stiffened plates and shells has been worked out by Farkas and Jármái (1997, 2003), and applied to uniaxially compressed plates and shells with stiffeners of various shapes Farkas and Jármái (2000) and biaxially compressed plates Farkas *et al.* (2005). Cost calculation, using different optimization techniques is an important topic to make the structure more competitive (Hadidi and Rafiee 2014), (Žula *et al.* 2016), (Kaveh *et al.* 2015). In these cases, mainly steel frame structures have been optimized. The cost calculations were different from the presented, because only those manufacturing costs have been considered in this paper, which have a direct effect on the sizes of the structure. Life cycle cost goes even further considering other essential cost elements (Kaveh *et al.* 2014). The application of robots and design their workplace is another important issue (Hazim and Jármái 2019).

The deflections due to lateral pressure, compression stress and the shrinkage of longitudinal welds are taken into account in the stress calculation and constraint. Furthermore, the local buckling constraint of the base plate strips is also formulated.

The cost function as the objective function includes two kinds of steel and three kinds of welding technologies. The design variables are the thickness of the base plate and the dimensions and the number of stiffeners.

The unique approach of this paper is that it considers both static and dynamic loadings with different load cycles, using different shape of stiffeners, different steel grades and employing optimization to determine the minimum mass and minimum cost structures.

2. Geometric characteristics and loadings

The geometric characteristics and loadings of stiffened

*Corresponding author, Professor, Ph.D.

E-mail: jarmai@uni-miskolc.hu

^a Ph.D., Associate Professor

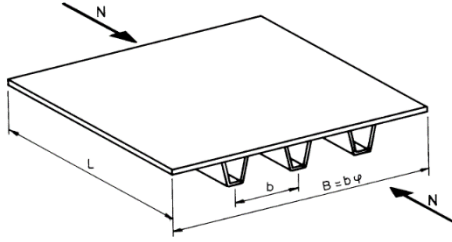


Fig. 1 Stiffened plate loaded by uniaxial compression

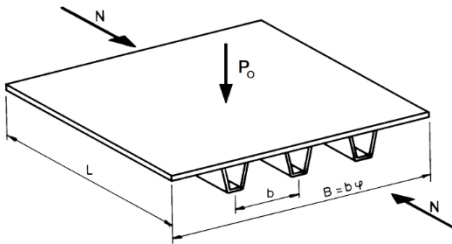


Fig. 2 Stiffened plate loaded by uniaxial compression and lateral pressure

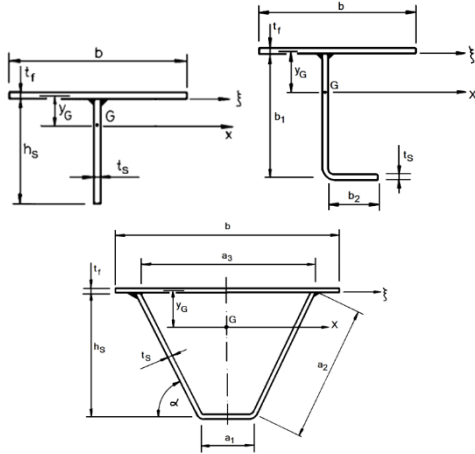


Fig. 3 Dimensions of the flat rib, L rib and trapezoidal ribs

plates are shown in Figs. 1 and 2. The figures show the direction of the N compression force and p_0 lateral pressure with the geometry of the stiffened plate: B base plate width, L base plate length, b the distance between stiffeners (effective slab width) and $\varphi = n + 1$ (n is the number of stiffeners). The stiffened plates are simply supported on all four edges.

Geometrical parameters of stiffened plates with flat ribs, L-shaped ribs and trapezoidal ribs can be seen in Fig. 3. The figures show G centre of mass of the stiffener and the effective slab width, y_G the distance between G and the centre line of the base plate and the geometry of stiffeners: t_s thickness of the stiffener, h_s height of the stiffener and special stiffener dimensions (b_1 , b_2 , a_1 , a_2 , a_3) and t_f thickness of the base plate.

The calculations of different geometrical parameters of the flat stiffener are:
stiffener cross-section

$$A_s = h_s t_s \quad (1)$$

stiffener height

$$h_s = 14 t_s \varepsilon \quad (2)$$

$$\varepsilon = \sqrt{235/f_y} \quad (3)$$

where f_y is the yield stress

$$y_G = \frac{h_s + t_f}{2} \frac{\delta_s}{1 + \delta_s} \quad (4)$$

where

$$\delta_s = \frac{A_s}{b t_f} \quad (5)$$

section moment of inertia

$$I_x = \frac{b t_f^3}{12} + b t_f y_G^2 + \frac{h_s^3 t_s}{12} + h_s t_s \left(\frac{h_s}{2} - y_G \right)^2 \quad (6)$$

stiffener moment of inertia

$$I_s = h_s^3 \frac{t_s}{3} \quad (7)$$

torsional moment of inertia

$$I_t = \frac{h_s t_s^3}{3} \quad (8)$$

warping constant

$$I_\omega = 0 \quad (9)$$

The calculations of different geometrical parameters of the L-stiffener are:

stiffener cross section

$$A_s = (b_1 + b_2) t_s \quad (10)$$

L-stiffener dimensions

$$b_1 = 30 t_s \varepsilon \quad (11)$$

$$b_2 = 12.5 t_s \varepsilon \quad (12)$$

$$y_G = \frac{b_1 t_s \frac{b_1 + t_f}{2} + b_2 t_s \left(b_1 + \frac{t_f}{2} \right)}{b t_f + A_s} \quad (13)$$

section moment of inertia

$$I_x = \frac{b t_f^3}{12} + b t_f y_G^2 + \frac{b_1^3 t_s}{12} + b_1 t_s \left(\frac{b_1}{2} - y_G \right)^2 + b_2 t_s (b_1 - y_G)^2 \quad (14)$$

stiffener moment of inertia

$$I_s = \frac{b_1^3 t_s}{3} + b_1^2 b_2 t_s \quad (15)$$

torsional moment of inertia

$$I_t = \frac{b_1 t_s^3}{3} + \frac{b_2 t_s^3}{3} \quad (16)$$

warping constant

$$I_{\omega} = \frac{b_1^2 b_2^3 t_s}{3} \quad (17)$$

The calculations of different geometrical parameters of the trapezoidal stiffener are:
stiffener cross-section

$$A_s = (a_1 + 2a_2)t_s \quad (18)$$

where (see Fig. 3)

$$a_2 = \sqrt{\left(\frac{a_3 - a_1}{2}\right)^2 + h h_s^2} \quad (19)$$

There are minimum values for $a_1 = 90$ and $a_3 = 300$ mm, thus stiffener height

$$h h_s = (a_2^2 - 105^2)^{1/2} \quad (20)$$

$$\sin^2 \alpha = 1 - \left(\frac{105}{a_2}\right)^2 \quad (21)$$

$$y_G = \frac{a_1 t_s (h h_s + t_f/2) + 2a_2 t_s (h h_s + t_f)/2}{b t_f + A_s} \quad (22)$$

section moment of inertia

$$I_x = \frac{b t_f^3}{12} + b t_f y_G^2 + a_1 t_s \left(h_s + \frac{t_f}{2} - y_G\right)^2 + \frac{1}{6} a_2^3 t_s \sin^2 \alpha + 2a_2 t_s \left(\frac{h_s + t_f}{2} - y_G\right)^2 \quad (23)$$

stiffener moment of inertia

$$I_s = a_1 h h_s^3 t_s + \frac{2}{3} a_2^3 t_s \sin^2 \alpha \quad (24)$$

torsional moment of inertia

$$I_t = \frac{4A_p^2}{\sum b_i/t_i} \quad (25)$$

where

$$A_p = h h_s \frac{a_1 + a_3}{2} = 195 h h_s \quad (26)$$

$$\sum \frac{b_i}{t_i} = \frac{a_1 + 2a_2}{t_s} + \frac{a_3}{t_f} \quad (27)$$

b is the distance between stiffeners, $\phi = n + 1$ (n is the number of stiffeners).

3. Design constraints in case of uniaxial compression

3.1 Global buckling calculation of stiffened plates

According to the method of Mikami and Niwa (1996), the effect of residual welding and initial imperfections stresses is considered by defining the buckling curves for a reduced slenderness (Fig. 4).

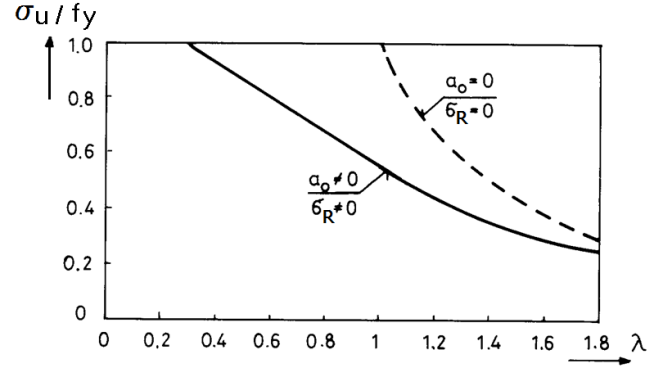


Fig. 4 Global buckling curve considering initial imperfections ($\alpha_0 \neq 0$) and residual welding stresses ($\sigma_R \neq 0$)

$$\lambda = (f_y / \sigma_{cr})^{1/2} \quad (28)$$

where f_y is the yield stress. The classical critical buckling stress for a uniaxially compressed longitudinally stiffened plate is

$$\sigma_{cr} = \frac{\pi^2 D}{h B^2} \left(\frac{1 + \gamma_S}{\alpha_R^2} + 2 + \alpha_R^2 \right) \text{ for } \alpha_R = L/B < \alpha_{R0} = (1 + \gamma_S)^{1/4} \quad (29)$$

$$\sigma_{cr} = \frac{2\pi^2 D}{h B^2} [1 + (1 + \gamma_S)^{1/2}] \text{ for } \alpha_R \geq \alpha_{R0}$$

where

$$\gamma_S = \frac{E I_S}{b D} \quad (30)$$

$$D = \frac{E t_f^3}{10.92} \quad (31)$$

where E is the Young modulus,
 B is the base plate width.

If the reduced slenderness is known, the actual global buckling stress (σ_U) can be calculated according to Mikami's method as follows

$$\frac{\sigma_U}{f_y} = 1 \text{ for } \lambda \leq 0.3$$

$$\frac{\sigma_U}{f_y} = 1 - 0.63(\lambda - 0.3) \text{ for } 0.3 \leq \lambda \leq 1 \quad (32)$$

$$\frac{\sigma_U}{f_y} = \frac{1}{(0.8 + \lambda^2)} \text{ for } \lambda > 1$$

The global buckling constraint is calculated as

$$\frac{N}{A} \leq \sigma_U \frac{\rho_P + \delta_S}{1 + \delta_S} \quad (33)$$

where

$$A = B t_f + (\phi - 1) A_s \quad (34)$$

$$\delta_S = \frac{A_s}{b t_f} \quad (35)$$

and ρ_P factor depends on the stresses, and it is as follows

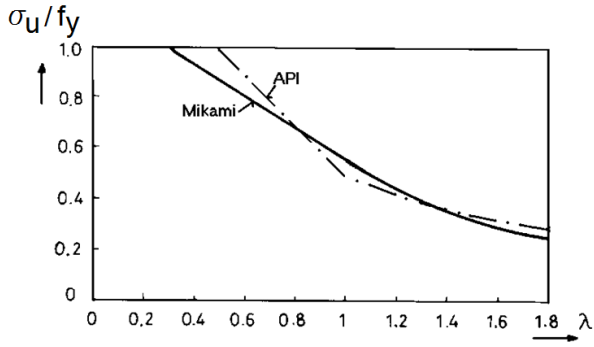


Fig. 5 Global buckling curve according to Mikami and API

$$\begin{aligned} \rho_P &= 1 \text{ if } \sigma_{UP} > \sigma_U \\ \rho_P &= \sigma_{UP}/f_f \text{ if } \sigma_{UP} < \sigma_U \end{aligned} \quad (36)$$

where σ_{UP} is according to Eq. (41).

According to API (1987)

$$\begin{aligned} \frac{\sigma_U}{f_y} &= 1 \text{ if } \lambda \leq 0.5 \\ \frac{\sigma_U}{f_y} &= 1.5 - \lambda \text{ if } 0.5 \leq \lambda \leq 1 \\ \frac{\sigma_U}{f_y} &= \frac{0.5}{\lambda} \text{ if } \lambda > 1 \end{aligned} \quad (37)$$

The global buckling constraint

$$\frac{N}{A} \leq \sigma_U \quad (38)$$

The differences in global buckling calculations between Mikami and API are visible in Fig. 5.

3.2 Single panel buckling calculation

This constraint eliminates local buckling of the base plate between the ribs. From the classical buckling formula, the critical stress (σ_{crP}) is calculated for simply supported ends and compressed in one direction

$$\sigma_{crP} = \frac{4\pi^2 E}{10.92} \left(\frac{t_F}{b} \right)^2 \quad (39)$$

The reduced slenderness is

$$\lambda_P = \left(\frac{4\pi^2 E}{10.92 f_y} \right)^{1/2} \frac{b}{t_F} = \frac{b/t_F}{56.8 \varepsilon}; \quad \varepsilon = \left(\frac{235}{f_y} \right)^{1/2} \quad (40)$$

and the actual local buckling stress considering residual welding stresses and initial imperfections is

$$\begin{aligned} \frac{\sigma_{UP}}{f_y} &= 1 \text{ for } \lambda_P \leq 0.526 \\ \frac{\sigma_{UP}}{f_y} &= \left(\frac{0.526}{\lambda_P} \right)^{0.7} \text{ for } \lambda_P > 0.526 \end{aligned} \quad (41)$$

The single panel buckling constraint is

$$\frac{N}{A} \leq \sigma_{UP} \quad (42)$$

3.3 Local and torsional buckling calculation of stiffeners

For open section stiffeners, the torsional buckling constraint is

$$\frac{N}{A} \leq \sigma_{UT} \quad (43)$$

where σ_{UT} is according to Eq. (46).

The classical torsional buckling stress is

$$\sigma_{crT} = \frac{GI_t}{I_S} + \frac{EI_\omega}{L^2 I_S} \quad (44)$$

where $G = E/2.6$ is the shear modulus, I_S is the polar moment of inertia, I_t is a torsional moment of inertia (Eqs. 8,16,25) and I_ω is warping constant (Eqs. 9,17). The actual torsional buckling stress is calculated in the function of reduced slenderness

$$\lambda_T = (f_y / \sigma_{crT})^{1/2} \quad (45)$$

$$\frac{\sigma_{UT}}{f_y} = 1 \text{ for } \lambda_T \leq 0.45$$

$$\frac{\sigma_{UT}}{f_y} = 1 - 0.53(\lambda_T - 0.45) \text{ for } 0.45 \leq \lambda_T \leq 1.41 \quad (46)$$

$$\frac{\sigma_{UT}}{f_y} = \frac{1}{\lambda_T^2} \text{ for } \lambda_T \geq 1.41$$

4. Design constraints for uniaxial compression and lateral pressure

4.1 Calculation of the deflection due to compression and lateral pressure

Paik *et al.* (2001) used differential equations of large deflection orthotropic plate theory and the Galerkin method to derive the following cubic equation for elastic deflection A_m of stiffened plate loaded by lateral pressure and uniaxial compression. They have continued this line for initial deflection in Kim *et al.* (2018).

$$C_1 A_m^3 + C_2 A_m^2 + C_3 A_m + C_4 = 0 \quad (47)$$

where

$$\begin{aligned} C_1 &= \frac{\pi^2}{16} \left(E_x \frac{m^4 B}{L^3} + E \frac{L}{B^3} \right); C_2 = \frac{3\pi^2 A_{om}}{16} \left(E_x \frac{m^4 B}{L^3} + E \frac{L}{B^3} \right) \\ C_3 &= \frac{\pi^2 A_{om}^2}{8} \left(E_x \frac{m^4 B}{L^3} + E \frac{L}{B^3} \right) + \frac{m^2 B}{L} \sigma_{xav} \\ &\quad + \frac{\pi^2}{t_F} \left(D_x \frac{m^4 B}{L^3} + 2H \frac{m^2}{LB} + D_y \frac{L}{B^3} \right) \end{aligned} \quad (48)$$

$$C_4 = A_{om} \frac{m^2 B}{L} \sigma_{xav} - \frac{16LB}{\pi^4 t_F} p$$

$$E_x = E \left(1 + \frac{nA_S}{Bt_F} \right); \quad E_y = E \quad (49)$$

where m is the number of half buckling length, $n = \varphi - 1$.

$$\sigma_{xav} = \frac{N}{Bt_f + (\phi - 1)A_s} \quad (50)$$

The self-weight is taken into account; consequently, the lateral pressure is modified as

$$p = p_0 + \frac{\rho V g}{BL} \quad (51)$$

where ρ is the material density and V is the volume of the structure, p_0 is the uniformly distributed load (Fig. 2), g is the gravitational constant, and A_{om} is according to Eq.(56). The torsional and flexural stiffnesses of the orthotropic plate are

$$D_x = \frac{Et_F^3}{12(1 - \nu_{xy}^2)} + \frac{Et_F y_G^2}{1 - \nu_{xy}^2} + \frac{EI_x}{b} \quad (52)$$

$$D_y = \frac{Et_F^3}{12(1 - \nu_{xy}^2)}$$

$$\nu_x = \frac{\nu}{0.86} \sqrt{\frac{\frac{E}{E_x} \left(\frac{Et_F^3}{12} + Et_F y_G^2 + \frac{EI_x}{b} \right) - \frac{Et_F^3}{12}}{\frac{EI_x}{b} \left(\frac{E}{E_x} \right)^2}} \quad (53)$$

$$\nu_y = \frac{E}{E_x} \nu_x; \quad \nu_{xy} = \sqrt{\nu_x \nu_y} \quad (54)$$

$$H = \frac{G_{xy} t_f}{b}; \quad G_{xy} = \frac{E}{2(1 + \nu_{xy})} \quad (55)$$

where ν is the Poisson coefficient.

The deflection due to lateral pressure is calculated as

$$A_{om} = \frac{5qL^4}{384EI_x}; \quad q = pb; \quad b = B/\phi \quad (56)$$

The solution of Eq. (47) is

$$A_m = -\frac{C_2}{3C_1} + k_1 + k_2 \quad (57)$$

where

$$k_1 = \sqrt[3]{-\frac{Y}{2} + \sqrt{\frac{Y^2}{4} + \frac{X^3}{27}}}; \quad k_2 = \sqrt[3]{-\frac{Y}{2} - \sqrt{\frac{Y^2}{4} + \frac{X^3}{27}}} \quad (58)$$

$$X = \frac{C_3}{C_1} - \frac{C_2^2}{3C_1^2}; \quad Y = \frac{2C_2^3}{27C_1^3} - \frac{C_2 C_3}{3C_1^2} + \frac{C_4}{C_1} \quad (59)$$

4.2 Deflection due to the shrinkage of longitudinal welds

The deflection of the stiffened plate due to the longitudinal welds is as follows

$$f_{max} = CL^2/8 \leq w_{max} = L/1000 \quad (60)$$

where the curvature for steel is

$$C = 0.844 * 10^{-3} Q_T y_T / I_x \quad (61)$$

where Q_T is the heat input and y_T is the weld eccentricity

$$y_T = y_G - t_f/2 \quad (62)$$

and I_x is the moment of inertia of cross-section containing a stiffener and a base plate strip of width b . The heat input for stiffeners is

$$Q_T = 2 * 59.5 a_w^2 \quad (63)$$

4.3 Calculation of stress constraint

The calculation of the stress constraint can include several effects of loads. These can be the following: average compression stress and bending stress caused by deflections due to lateral pressure, compression and shrinkage of longitudinal welds.

$$\sigma_{max} = \sigma_{xav} + \frac{M}{I_x} y_G \leq \sigma_{UP} \quad (64)$$

where M is the bending moment

$$M = N(A_{om} + A_m + f_{max}) + \frac{qL^2}{8} \quad (65)$$

σ_{xav} is according to Eq. (50).

According to Mikami and Niwa (1996) the calculation of local buckling strength of a face plate strip of width

$$b_1 = \max(a_3, b - a_3) \quad (66)$$

This is calculated taking into account the effect of residual welding stresses and initial imperfections

$$\sigma_{UP} = f_y \quad \text{when } \lambda_p \leq 0.526 \quad (67)$$

$$\sigma_{UP} = \left(\frac{0.526}{\lambda_p} \right)^{0.7} \quad \text{when } \lambda_p \geq 0.526$$

where

$$\lambda_p = \left(\frac{4\pi^2 E}{10.92 f_y} \right)^{1/2} \frac{b_1}{t_f} = \frac{b_1/t_f}{56.8\epsilon} \quad (68)$$

5. The objective function and the optimization technique

5.1 Cost function

The objective function to be minimized – the cost – is defined as the sum of material and fabrication costs

$$K = K_m + K_f = k_m \rho V + k_f \sum T_i \quad (69)$$

and in another formula

$$\frac{K}{k_m} = \rho V + \frac{k_f}{k_m} (T_1 + T_2 + T_3) \quad (70)$$

where ρ is the material density and V is the volume of the structure. K_m and K_f are material and fabrication costs in \$, k_m and k_f are the specific material and fabrication costs in \$/kg, and \$/min. T_i is the fabrication time, which can be calculated as follows:

Table 1 Welding times in the function of the weld size a_w for longitudinal fillet welds in downhand position

| Welding technology | a_w mm | $10^3 C_2 a_w^n$ |
|-------------------------------------------------|-------------|------------------|
| SAW Submerged Arc Welding | 0-15 | $0.2349 a_w^2$ |
| SMAW Gas Metal Arc Welding with CO ₂ | 0-15 | $0.3258 a_w^2$ |
| GMAW Shielded Metal Arc Welding | 0-15 | $0.7889 a_w^2$ |

- T_1 is the time for preparation, assembly and tacking

$$T_1 = \theta_d \sqrt{\kappa \rho V} \quad (71)$$

where θ_d is a difficulty factor which expresses the complexity of the welded structure, κ is the number of assembled structural elements,

- T_2 is the time of welding

$$T_2 = \sum C_{2i} a_{wi}^n L_{wi} \quad (72)$$

where L_{wi} is the length of welds. The values of $C_{2i} a_{wi}^n$ can be obtained from formulae or diagrams constructed using the COSTCOMP (1990) software, a_w is the dimension of the weld. The value of a_w should be the maximum of $0.5t_f$ (rounded to mm) or 4 mm. The values for three major welding technologies are given in Table 1.

- T_3 is the time of additional work such as deslagging, changing electrodes and chipping.

$T_3 \approx 0.3T_2$ thus

$$T_2 + T_3 = 1.3 \sum C_{2i} a_{wi}^n L_{wi} \quad (73)$$

The total time for welding is the sum of T_1 , T_2 , and T_3 (Farkas and Jármai 2013).

The investment cost of the production equipment is not considered, because they can be used for other productions in their lifetime. The design, inspection and maintenance costs are usually proportional to the mass of the structure. That is why they are not included in the cost function.

5.2 The Rosenbrock's Hillclimb optimization method

This mathematical programming method is used in this study to minimize the cost function (Rosenbrock 1960). It is a direct search numerical method without derivatives. The iterative algorithm of the method is based on the Hooke and Jeeves (1961) searching method. It starts with the given initial values. During the search, it takes small steps in the direction of orthogonal coordinates. In order to determine discrete values, the algorithm is modified so that a secondary search is carried out. The procedure stops the search for the optimum when the iteration number reaches its limit, or the convergence criterion is satisfied. In our calculations, in most cases the convergence criterion fulfilled. A strict convergence limit was given, the 10^{-8} portion of the actual objective function. It generally prevents us from finding local minima. The technique is a continuous one, where the discretization is made after finding the continuous optimum. The discretization is described in Farkas and Jármai (1997). The deterministic

algorithm solves constrained problems in our cases. Using the multiple starting point technique, one can be sure that the global optimum is found.

During our calculations the iteration number varies 500-2000, depending on the convergence criteria. The convergence criteria were 10^{-5} - 10^{-8} .

6. Numerical data and optimum results of static loads

6.1 Longitudinally stiffened plate loaded by a uniaxial compression

The given data are: base plate width $B = 6000$ mm, base plate length $L = 3000$ mm, compression force $N = 1.974 \times 10^7$ N, material density $\rho = 7.85 \times 10^{-6}$ kg/mm³, Young's modulus $E = 2.1 \times 10^5$ MPa, and yield stress $f_y = 355$ MPa, the Poisson coefficient is 0.3. The design variables, the thicknesses of the base plate and stiffeners and the number of ribs, are limited in range (Eq. 74). If the k_F/k_m ratio is zero, we do not consider fabrication cost, and the optimum result is mass minimum. Thus, the mass minimum does not depend on welding technology. That is why mass minimum is the same, and so it is not shown in Tables 4–7.

$$3 \leq t_f \leq 40 \text{ mm}$$

$$3 \leq t_s \leq 12 \text{ mm} \quad (74)$$

$$4 \leq \phi \leq 10$$

Tables 2 and 3 show the optimum dimensions for SAW technology, Tables 4 and 5 for SMAW and Tables 6 and 7 for GMAW.

The results for cost function are, according to Eq. (69) and the considered constraints are according to Eqs. (38, 42, 43).

Table 2 Optimized dimensions with **L-shaped** stiffener (SAW)

| | k_F/k_m | t_f mm | t_s mm | ϕ | K/k_m kg |
|--------|-----------|-------------|-------------|--------|---------------|
| Mikami | 0 | 18 | 7 | 9 | 2936 |
| | 1 | 18 | 7 | 9 | 3658 |
| | 2 | 19 | 7 | 8 | 4373 |
| API | 0 | 17 | 7 | 10 | 2844 |
| | 1 | 17 | 7 | 10 | 3614 |
| | 2 | 19 | 7 | 8 | 4373 |

Table 3 Optimized dimensions with **trapezoidal** stiffener (SAW)

| | k_F/k_m | t_f mm | t_s mm | ϕ | K/k_m kg |
|--------|-----------|-------------|-------------|--------|---------------|
| Mikami | 0 | 18 | 6 | 6 | 2930 |
| | 1 | 18 | 6 | 6 | 3474 |
| | 2 | 18 | 6 | 6 | 4018 |
| API | 0 | 15 | 6 | 8 | 2660 |
| | 1 | 15 | 6 | 8 | 3303 |
| | 2 | 15 | 6 | 8 | 3946 |

Table 4 Optimized dimensions with **L-shaped** stiffener (SMAW)

| | k_F/k_m | t_f mm | t_s mm | ϕ | K/k_m kg |
|--------|-----------|-------------|-------------|--------|---------------|
| Mikami | 1 | 19 | 7 | 8 | 4184 |
| | 2 | 19 | 7 | 8 | 5341 |
| API | 1 | 19 | 7 | 8 | 4185 |
| | 2 | 21 | 8 | 6 | 5115 |

Table 5 Optimized dimensions with **trapezoidal** stiffener (SMAW)

| | k_F/k_m | t_f mm | t_s mm | ϕ | K/k_m kg |
|--------|-----------|-------------|-------------|--------|---------------|
| Mikami | 1 | 18 | 6 | 6 | 3820 |
| | 2 | 18 | 6 | 6 | 4710 |
| API | 1 | 15 | 6 | 8 | 3787 |
| | 2 | 15 | 6 | 8 | 4914 |

Table 6 Optimized dimensions with **L-shaped** stiffener (GMAW)

| | k_F/k_m | t_f mm | t_s mm | ϕ | K/k_m kg |
|--------|-----------|-------------|-------------|--------|---------------|
| Mikami | 1 | 18 | 7 | 9 | 3749 |
| | 2 | 19 | 7 | 8 | 4532 |
| API | 1 | 17 | 7 | 10 | 3716 |
| | 2 | 19 | 7 | 8 | 4532 |

Table 7 Optimized dimensions with **trapezoidal** stiffener (GMAW)

| | k_F/k_m | t_f mm | t_s mm | ϕ | K/k_m kg |
|--------|-----------|-------------|-------------|--------|---------------|
| Mikami | 1 | 18 | 6 | 6 | 3531 |
| | 2 | 18 | 6 | 6 | 4132 |
| API | 1 | 15 | 6 | 8 | 3382 |
| | 2 | 15 | 6 | 8 | 4104 |

In all cases, **trapezoidal** stiffeners are better than **L-shaped** stiffeners. The mass savings are between 5 and 10 %.

6.2 Longitudinally stiffened plate loaded by a uniaxial compression and lateral pressure

In the following calculation, stiffened plates with L and trapezoidal ribs are compared. The given data are: base plate width $B = 4000$ mm, base plate length $L = 6000$ mm, compression force $N = 1.974 \times 10^7$ N. The Young's modulus is $E = 2.1 \times 10^5$ MPa, material density is $\rho = 7.85 \times 10^{-6}$ kg/mm³. In the calculation, there are values of lateral pressures $p_0 = 0.005, 0.01, 0.02$ MPa and stresses $f_y = 255, 355$ MPa. The applied welding technology is GMAW. The design variables, the thicknesses of base plate and stiffener and the number of ribs, are limited in range (Eq. 75). The results are shown in Tables 8–11. The optimum results are marked by bold letters.

$$\begin{aligned}
 3 &\leq t_f \leq 40 \text{ mm} \\
 3 &\leq t_s \leq 12 \text{ mm} \\
 4 &\leq \phi \leq 10
 \end{aligned}
 \tag{75}$$

The results for cost function are, according to Eq. (69) and the considered constraints are according to Eqs. (38, 42, 43, 60, 64).

Table 8 Optimized dimensions with **L-shaped** stiffener $k_F/k_m=0$, the material minima

| f_y MPa | p_0 MPa | t_f mm | t_s mm | ϕ | K/k_m kg | |
|--------------|--------------|-------------|-------------|--------|---------------|---------------|
| | | | | | $k_F/k_m=0$ | $k_F/k_m=1.5$ |
| 235 | 0.02 | 23 | 12 | 6 | 5774 | 7984 |
| 235 | 0.01 | 21 | 12 | 6 | 5398 | 7580 |
| 235 | 0.005 | 22 | 10 | 6 | 5146 | 6889 |
| 355 | 0.02 | 22 | 12 | 6 | 5849 | 8025 |
| 355 | 0.01 | 20 | 12 | 6 | 5435 | 7582 |
| 355 | 0.005 | 19 | 10 | 8 | 5192 | 7400 |

Table 9 Optimized dimensions with **L-shaped** stiffener $k_F/k_m=1.5$, the material minima

| f_y MPa | p_0 MPa | t_f mm | t_s mm | ϕ | K/k_m kg | |
|--------------|--------------|-------------|-------------|--------|---------------|---------------|
| | | | | | $k_F/k_m=0$ | $k_F/k_m=1.5$ |
| 235 | 0.02 | 26 | 11 | 5 | 5867 | 7560 |
| 235 | 0.01 | 29 | 9 | 4 | 5950 | 7107 |
| 235 | 0.005 | 26 | 8 | 5 | 5411 | 6639 |
| 355 | 0.02 | 27 | 11 | 4 | 6246 | 7616 |
| 355 | 0.01 | 26 | 10 | 4 | 5926 | 7158 |
| 355 | 0.005 | 24 | 8 | 5 | 5432 | 6627 |

Table 10 Optimized dimensions with **trapezoidal** stiffener $k_F/k_m=0$, the material minima

| f_y MPa | p_0 MPa | t_f mm | t_s mm | ϕ | K/k_m kg | |
|--------------|--------------|-------------|-------------|--------|---------------|---------------|
| | | | | | $k_F/k_m=0$ | $k_F/k_m=1.5$ |
| 235 | 0.02 | 17 | 11 | 5 | 5122 | 6764 |
| 235 | 0.01 | 17 | 10 | 5 | 4804 | 6264 |
| 235 | 0.005 | 18 | 9 | 5 | 4704 | 6011 |
| 355 | 0.02 | 15 | 10 | 6 | 4944 | 6635 |
| 355 | 0.01 | 15 | 9 | 6 | 4616 | 6102 |
| 355 | 0.005 | 15 | 8 | 6 | 4320 | 5621 |

Table 11 Optimized dimensions with **trapezoidal** stiffener $k_F/k_m=1.5$, the material minima

| f_y MPa | p_0 MPa | t_f mm | t_s mm | ϕ | K/k_m kg | |
|--------------|--------------|-------------|-------------|--------|---------------|---------------|
| | | | | | $k_F/k_m=0$ | $k_F/k_m=1.5$ |
| 235 | 0.02 | 23 | 9 | 4 | 5317 | 6437 |
| 235 | 0.01 | 23 | 8 | 4 | 5122 | 6132 |
| 235 | 0.005 | 22 | 8 | 4 | 4934 | 5932 |
| 355 | 0.02 | 17 | 10 | 5 | 4991 | 6431 |
| 355 | 0.01 | 18 | 8 | 5 | 4700 | 5845 |
| 355 | 0.005 | 15 | 8 | 6 | 4320 | 5621 |

Using the multiple starting point technique, one can be sure that the global optimum is found. The results of Sections 6.1 and 6.2 show that the trapezoidal stiffener is the most economic one. The cost saving can be around 20 % comparing the optima with flat, or L-shaped ribs. In general, the method of Mikami gives thinner basic plates compared to that of the API. Materials with higher yield stress give cheaper results. The cost savings can reach 40%, although the higher strength steel is 8-10% more expensive. Generally, the material and cost minima are different, and the number of ribs is smaller at cost minima due to the welding cost effects. If we do not consider the investment cost, SAW is the cheapest welding process.

For uniaxially and laterally loaded plates the ratio between material and welding cost is from 13% (flat stiffener, higher yield stress and minimum lateral pressure) to 64% (trapezoidal stiffener, lower yield stress and maximum lateral pressure). The number of stiffeners φ decreases if the lateral pressure is increased, but φ increases if the yield stress of the material is increased.

7. Overview of various fatigue designs for compressed stiffened plates

In recent decades, engineering knowledge has changed, which has heavily influenced the design of welded structures. Fatigue can play a significant effect on the behaviour of the structure (Georgioudakis *et al.* 2017). New materials and new welding technologies have come into use. Therefore, it is essential to optimize the cost of different structures for the various options (Virág 2006) carried out to approximate the behaviour of structures by various research institutes, universities and industrial laboratories. Fatigue test equipment has improved as well, allowing a higher number of cycles.

7.1 Factors influencing the fatigue of welded joints

It is essential to take several factors into account in weld design. The following items should be considered: the raw material used; welding technology; residual stresses; the type of bond; the weld geometry; welding failures; the voltage ranges; and the number of cycles. According to the current fatigue behaviour standards, the $\Delta\sigma - N$ curve can be regarded as the fatigue value being unchanged after only $N = 10^8$ or 10^9 cycles. In most cases, the stress condition is a combination of normal stress and shear stress. The fatigue behaviour can vary significantly with the changes in these factors.

7.2 Fatigue design according to Eurocode 3

Welded joints are rated by Eurocode 3 (2005). The class number $\Delta\sigma_C, \Delta\tau_C$ means the reference value of the fatigue strength in MPa at $N = 2 \cdot 10^6$ cycles. In the case of N cycles, the values of fatigue stress range $\Delta\sigma_N, \Delta\tau_N$ are given graphically (straight lines in a log-log coordinate system, Fig. 6). The different categories are represented by parallel lines from 36 MPa to 160 MPa in the corresponding figure of the standard.

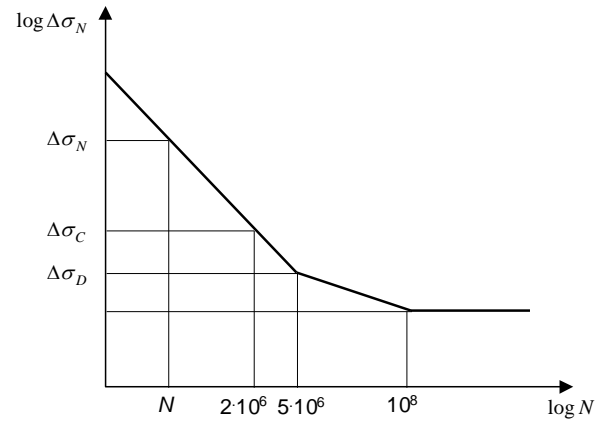


Fig. 6 EC3 recommendations: Fatigue resistance S-N curve

In Fig. 6 there is only one line drawn, but the calculation is the same for any of the categories. Accordingly, the values $\Delta\sigma_N, \Delta\tau_N$ can be determined by linear interpolation (Eqs. 76, 77, 78) if $\Delta\sigma_C, m$, and N are known. The number of cycles N may vary between 10^5 and infinite. The fatigue boundary values of the normal stress are dependent on the cycles.

If $N \leq 5 \cdot 10^6$ then

$$\log \Delta \sigma_N = \frac{1}{m} \log \frac{2 \cdot 10^6}{N} + \log \Delta \sigma_C \quad (76)$$

where m is the slope of the fatigue strength curve, $m = 3$, $\Delta\sigma_C$ is the fatigue stress range at $N=2 \cdot 10^6$ cycles. This stress corresponds to the value of the joint group (between 36 and 160 MPa).

If $5 \cdot 10^6 \leq N \leq 10^8$ then

$$\log \Delta \sigma_N = \frac{1}{m} \log \frac{5 \cdot 10^6}{N} + \log \Delta \sigma_D \quad (77)$$

where the slope is smaller, $m = 5$, $\Delta\sigma_D$ is the fatigue stress range at $N=5 \cdot 10^6$ cycles (this can be determined from the value of $\Delta\sigma_C$).

$$\log \Delta \tau_N = \frac{1}{m} \log \frac{2 \cdot 10^6}{N} + \log \Delta \tau_C \quad (78)$$

where m is the slope of the fatigue strength curve, $m = 5$, $\Delta\tau_C$ is the fatigue stress range at $N=2 \cdot 10^6$ cycles.

The interaction formula of the EC3 standard in the case of combined stress (where $\Delta\sigma, \Delta\tau$ are the normal and shear stress for designing, $\Delta\sigma_N, \Delta\tau_N$ are the fatigue stress amplitudes, γ_{Ff} and γ_{Mf} partial safety factors for fatigue loads and strengths) is

$$\left(\frac{\gamma_{Ff} \Delta \sigma}{\Delta \sigma_N / \gamma_{Mf}} \right)^3 + \left(\frac{\gamma_{Ff} \Delta \tau}{\Delta \tau_N / \gamma_{Mf}} \right)^5 \leq 1 \quad (79)$$

In the ENV 1991 Eurocode 1 the fatigue loads already contain the value of the γ_{Ff} safety factor. Usually, the value of γ_{Ff} is assumed to be 1.

The recommended values for γ_{Mf} safety factors are given in Table 12 (Eurocode 3 2005). "Low consequence" means that a local failure will not result in failure of the

Table 12 Recommended values for partial factors γ_{Mf}

| Assessment method | Consequence of failure | |
|-------------------|------------------------|------------------|
| | Low consequence | High consequence |
| Damage tolerant | 1.00 | 1.15 |
| Safe life | 1.15 | 1.35 |

Table 13 Classification of welding technologies

| Welding technology | EC3 | IIW |
|--------------------|-------------------------|-------------------------|
| | $\Delta\sigma_c$ MPa | $\Delta\sigma_c$ MPa |
| SMAW | 100 | 90 |
| GMAW | 112 | 100 |
| SAW | 125 | 125 |

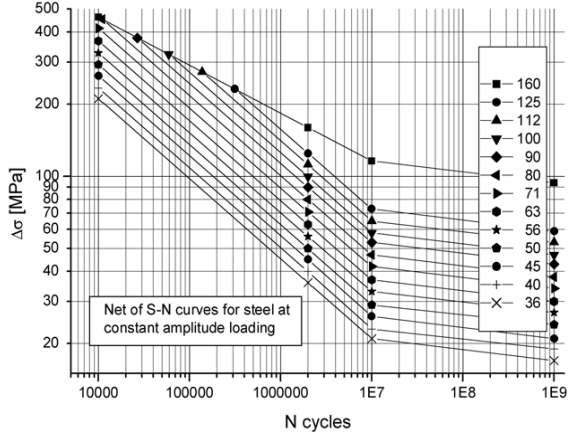


Fig. 7 IIW recommendations: Fatigue resistance S-N curves

entire structure, while “high consequence” means that a local failure will result in failure of the whole structure. We calculate with a value of 1.15 in the numerical example.

7.3 Fatigue design according to the International Institute of Welding

The International Institute of Welding (IIW) has developed recommendations for the determination of fatigue of welded connections (Recommendations (2008)). The advantage of the recommendation is the use of new research results, and it is valid up to 960 MPa yield stress, compared to the 690 MPa in Eurocode. It gives the fatigue strength, not only for steel but for aluminium. The fatigue strength is constant over 10^9 cycles (Fig. 7).

If $N \leq 10^7$ then

$$\log \Delta \sigma_N = \frac{1}{m} \log \frac{2 * 10^6}{N} + \log \Delta \sigma_C \quad (80)$$

where m is the slope of the curve is constant, $m = 3$, $\Delta \sigma_C$ is the fatigue stress range at $N=2*10^6$ cycles. This stress corresponds to the value of the joint group (between 36 and 160 MPa).

If $10^7 \leq N$ then

$$\log \Delta \sigma_N = \frac{1}{m} \log \frac{10^7}{N} + \log \Delta \sigma_D \quad (81)$$

where the slope is smaller, $m = 5$, $\Delta \sigma_D$ is the fatigue stress range at $N=10^7$ cycles (this can be determined from the value of $\Delta \sigma_C$).

$$\log \Delta \tau_N = \frac{1}{m} \log \frac{2 * 10^6}{N} + \log \Delta \tau_C \quad (82)$$

where m is the slope of the fatigue strength curve, $m = 5$, $\Delta \tau_C$ is the fatigue stress range at $N=2*10^6$ cycles.

7.4 Numerical example for fatigue design

The fatigue constraint has been calculated based on EC standards and IIW recommendations. Three kinds of welding techniques are also investigated. Different welding technologies are classified in various weld fatigue ranges according to Table 13. Other design constraints are calculated according to the Mikami method (see Section 3): global buckling (Eq. 38), single panel buckling (Eq. 42), local and torsional buckling (Eq. 43) of stiffeners.

Given data: $B = 6000$ mm, $L = 4000$ mm, $N = 1.2 \times 10^7$ N, $f_y = 235$ MPa, $E = 2.1 \times 10^5$ MPa, $G = E/2.6$, $\rho = 7.85 \times 10^6$ kg/mm³, $\Theta_d = 3$. The considered numbers of cycles are $<10^4$, 10^5 , 10^6 , 10^7 and 10^8 . If the number of cycles is less than 10^4 it is outside the range of validity in the fatigue design standard. The design variables – the thicknesses of the base plate and the stiffener and the number of the ribs – are limited in a range (Eq. 83). Results are shown in Tables 14–16.

$$3 \leq t_f \leq 40 \text{ mm}$$

$$3 \leq t_s \leq 30 \text{ mm} \quad (83)$$

$$4 \leq \phi \leq 10$$

The objective function is the cost function to minimize. It is defined as the sum of material and fabrication costs.

$$K = K_m + K_f = k_m \rho V + k_f \sum T_i \quad (84)$$

5. Conclusions

As we stated at the beginning, the main requirements of modern welded metal structures are the load-carrying capacity (safety), fitness for production, and economy. These requirements can be met by structural optimization: the economy is achieved by minimizing the cost function. The safety and fitness for production are guaranteed by fulfilling the design and fabrication constraints. The cost function includes the material and the welding costs, using different steel grades and different welding technologies. The Hillclimb nonlinear optimization technique was useful finding the optimum sizes of the stiffened plates.

At the static uniaxially loaded plates calculations, the cost saving can be around 20 % comparing the optima with flat, or L-shaped ribs. In general, the method of Mikami gives thinner basic plates compared to that of the API (~4 %). Materials with higher yield stress give cheaper results. The cost savings can be up to 40 %, even though the higher strength steel is 5-10 % more expensive. Generally, the material and cost minima are different, and the number of

Table 14 Results for SMAW technology

| SMAW | k_f/k_m | t_f mm | t_s mm | φ | K/k_m kg |
|------------------|-----------|-------------|-------------|-----------|---------------|
| N cycles | 0 | 5 | 10 | 29 | 2172 |
| <10 ⁴ | 1 | 17 | 14 | 5 | 5555 |
| | 2 | 17 | 14 | 5 | 7562 |
| | 0 | 5 | 10 | 29 | 2172 |
| EC3 | 1 | 17 | 14 | 5 | 5555 |
| 10 ⁵ | 2 | 17 | 14 | 5 | 7562 |
| | 0 | 11 | 16 | 24 | 4660 |
| EC3 | 1 | 24 | 14 | 4 | 6400 |
| 10 ⁶ | 2 | 24 | 14 | 4 | 8021 |
| | 0 | 26 | 15 | 26 | 7371 |
| EC3 | 1 | 39 | 11 | 4 | 8771 |
| 10 ⁷ | 2 | 39 | 11 | 4 | 10036 |
| | 0 | 31 | 23 | 26 | 11654 |
| EC3 | 1 | 40 | 28 | 13 | 32137 |
| 10 ⁸ | 2 | 40 | 28 | 13 | 52603 |
| | 0 | 5 | 10 | 29 | 2172 |
| IIW | 1 | 18 | 14 | 4 | 5218 |
| 10 ⁵ | 2 | 18 | 14 | 4 | 6787 |
| | 0 | 10 | 19 | 16 | 4264 |
| IIW | 1 | 21 | 14 | 4 | 5810 |
| 10 ⁶ | 2 | 21 | 14 | 4 | 7406 |
| | 0 | 10 | 24 | 29 | 8973 |
| IIW | 1 | 40 | 29 | 5 | 16551 |
| 10 ⁷ | 2 | 40 | 29 | 5 | 24088 |
| | 0 | 40 | 29 | 19 | 14190 |
| IIW | 1 | 40 | 29 | 19 | 46798 |
| 10 ⁸ | 2 | 40 | 30 | 18 | 80066 |

ribs is smaller at cost minima due to the welding cost effects. If we do not consider the investment cost, submerged arc welding is the cheapest welding process.

For uniaxially and laterally loaded plates the ratio between material and welding cost is from 13 % (flat stiffener, higher yield stress and minimum lateral pressure) to 64 % (trapezoidal stiffener, lower yield stress and maximum lateral pressure). The number of stiffeners ($n=\varphi-1$) decreases if the lateral pressure is increased, but φ increases if the yield stress of the material is increased. There is a limit for the maximum number of stiffeners to be able to make the welding to the baseplate. This limit is 300 mm and all solutions fulfil this requirement.

At dynamic loading, the results show the high influence of the number of cycles on fatigue and the optimal sizes of the stiffened plates. The dimensions and the number of ribs increase with the number of cycles, of course. The fatigue constraint is activated at around 10⁶ cycles. Material cost optimization results in a higher number of ribs. In total cost optimization, the dimensions increase first, then the number of ribs. Comparisons show that it is worth considering both the technology and the costs of the structure and optimizing them in the design phase.

In the case of 10⁵ cycles and at lower ranges, the fatigue constraints are not activated; therefore, Eurocode and IIW calculations give the same results. At 10⁶ cycles, the

Table 15 Results for GMAW technology

| GMAW | k_f/k_m | t_f mm | t_s mm | φ | K/k_m kg |
|------------------|-----------|-------------|-------------|-----------|---------------|
| N cycles | 0 | 5 | 10 | 29 | 2172 |
| <10 ⁴ | 1 | 11 | 12 | 10 | 4227 |
| | 2 | 15 | 13 | 6 | 5460 |
| | 0 | 5 | 10 | 29 | 2172 |
| EC3 | 1 | 11 | 12 | 10 | 4227 |
| 10 ⁵ | 2 | 15 | 13 | 6 | 5460 |
| | 0 | 16 | 16 | 11 | 4139 |
| EC3 | 1 | 21 | 14 | 4 | 5102 |
| 10 ⁶ | 2 | 21 | 14 | 4 | 5990 |
| | 0 | 6 | 21 | 29 | 6558 |
| EC3 | 1 | 34 | 12 | 4 | 7449 |
| 10 ⁷ | 2 | 34 | 12 | 4 | 8301 |
| | 0 | 40 | 21 | 16 | 10443 |
| EC3 | 1 | 40 | 29 | 9 | 17114 |
| 10 ⁸ | 2 | 40 | 29 | 9 | 23735 |
| | 0 | 5 | 10 | 29 | 2172 |
| IIW | 1 | 11 | 12 | 10 | 4227 |
| 10 ⁵ | 2 | 15 | 13 | 6 | 5460 |
| | 0 | 18 | 13 | 6 | 3762 |
| IIW | 1 | 19 | 14 | 4 | 4707 |
| 10 ⁶ | 2 | 19 | 14 | 4 | 5577 |
| | 0 | 7 | 23 | 30 | 8063 |
| IIW | 1 | 40 | 20 | 4 | 9618 |
| 10 ⁷ | 2 | 40 | 20 | 4 | 11174 |
| | 0 | 17 | 28 | 29 | 12852 |
| IIW | 1 | 40 | 24 | 22 | 24694 |
| 10 ⁸ | 2 | 39 | 30 | 15 | 36870 |

Eurocode solution is more expensive, but in the case of 10⁷ and 10⁸ it becomes cheaper compared to the IIW results due to the thickness limitations.

If the number of cycles increases 10, 100, 1000 times, this increases the cost of the stiffened plate by 100, 200, 400%, respectively.

Comparisons show that the application of optimization is beneficial since it is possible to reduce the cost of the structure by 15-25%. If we compare non-optimized versions, in that case the cost saving can be even higher.

The main conclusion is that the optimum sizes depend on the welding technology, the material yield stress, the profile of the stiffeners, the load cycles and the place of the production (labour costs).

Acknowledgments

The research was supported by the EFOP-3.6.1-2016-16-00011 “Younger and Renewing University – Innovative Knowledge City – institutional development of the University of Miskolc aiming at intelligent specialisation” project implemented in the framework of the Széchenyi 2020 program. The realization of this project is supported by the European Union, co-financed by the European Social Fund.

Table 16 Results for SAW technology

| SAW | k_f/k_m | t_f mm | t_s mm | φ | K/k_m kg |
|------------------|-----------|-------------|-------------|-----------|---------------|
| N cycles | 0 | 5 | 10 | 29 | 2172 |
| <10 ⁴ | 1 | 11 | 12 | 10 | 3921 |
| | 2 | 15 | 13 | 6 | 5060 |
| | 0 | 5 | 10 | 29 | 2172 |
| EC3 | 1 | 11 | 12 | 10 | 3921 |
| 10 ⁵ | 2 | 15 | 13 | 6 | 5060 |
| | 0 | 15 | 9 | 28 | 3787 |
| EC3 | 1 | 19 | 14 | 4 | 4568 |
| 10 ⁶ | 2 | 19 | 14 | 4 | 5299 |
| | 0 | 30 | 13 | 4 | 5874 |
| EC3 | 1 | 30 | 13 | 4 | 6644 |
| 10 ⁷ | 2 | 30 | 13 | 4 | 7413 |
| | 0 | 40 | 17 | 15 | 9314 |
| EC3 | 1 | 40 | 26 | 7 | 12562 |
| 10 ⁸ | 2 | 40 | 26 | 7 | 15805 |
| | 0 | 5 | 10 | 29 | 2172 |
| IHW | 1 | 11 | 12 | 10 | 3921 |
| 10 ⁵ | 2 | 15 | 13 | 6 | 5060 |
| | 0 | 8 | 11 | 29 | 2996 |
| IHW | 1 | 15 | 13 | 6 | 4129 |
| 10 ⁶ | 2 | 15 | 13 | 6 | 5060 |
| | 0 | 6 | 22 | 26 | 6449 |
| IHW | 1 | 34 | 12 | 4 | 7346 |
| 10 ⁷ | 2 | 34 | 12 | 4 | 8097 |
| | 0 | 39 | 27 | 10 | 10231 |
| IHW | 1 | 40 | 30 | 8 | 15014 |
| 10 ⁸ | 2 | 40 | 30 | 8 | 19723 |

References

- American Petroleum Institute API (1987), Bulletin on design of flat plate structures. Bulletin 2V. Washington.
- Bourada M., A. Bouadi, A.A. Bousahla, A. Senouci, F. Bourada, A. Tounsi and S.R. Mahmoud (2019), "Buckling behavior of rectangular plates under uniaxial and biaxial compression", *Struct. Eng. Mech.*, **70**(1), 113-123. <https://doi.org/10.12989/sem.2019.70.1.113>
- COSTCOMP (1990), Programm zur Berechnung der Schweisskosten. Deutscher Verlag für Schweißtechnik, Düsseldorf.
- Eurocode 3 (2005), Design of Steel Structures -Part 1-9: Fatigue; European Committee for Standardization (CEN).
- Faiza K., D. Lamia, S. Mohamed, T. Abdelouahed and Mahmoud S.R. (2017), "An original single variable shear deformation theory for buckling analysis of thick isotropic plates", *Struct. Eng. Mech.*, **63**(4), 439-446. <https://doi.org/10.12989/sem.2017.63.4.439>
- Farkas J., Jármai K. (1997), *Analysis and Optimum Design of Metal Structures*. Balkema, Rotterdam-Brookfield.
- Farkas J., Jármai K. (2000), "Minimum cost design and comparison of uniaxially compressed plates with welded flat-, L- and trapezoidal stiffeners", *Welding in the World*, **44**(3), 47-51.
- Farkas J., Jármai K. (2003), *Economic Design of Metal Structures*, Millpress, Rotterdam.
- Farkas J., Simoes M.C. and Jármai K. (2005), "Minimum cost design of a welded stiffened square plate loaded by biaxial compression", *Struct. Multidisciplinary Optimization*, **29**(4), 298-303. <https://doi.org/10.1007/s00158-004-0385-0>.
- Farkas J., Jármai K. (2013), *Optimum Design of Steel Structures*, Springer Verlag, Heidelberg, Germany.
- Fernandes G.R. and Neto J.R. (2015), "Analysis of stiffened plates composed by different materials by the boundary element method", *Struct. Eng. Mech.*, **56**(4), 605-623. <https://doi.org/10.12989/sem.2015.56.4.605>
- Georgioudakis M., Lagaros N.D. and Papadrakakis M. (2017), "Probabilistic shape design optimization of structural components under fatigue", *Comput. Struct.*, **182**, 252-266. <https://doi.org/10.1016/j.compstruc.2016.12.008>
- Hadidi A. and Rafiee A. (2014), "Harmony search based, improved Particle Swarm Optimizer for minimum cost design of semi-rigid steel frames", *Struct. Eng. Mech.*, **50**(3), 323-347. <https://doi.org/10.12989/sem.2014.50.3.323>
- Hazim G. N., Jármai K. (2019), "Kinematic-based structural optimization of robots", *Pollack Periodica* **14**(3), 213-222. <https://doi.org/10.1556/606.2019.14.3.20>
- Hooke, R.; Jeeves, T.A. (1961), "'Direct search' solution of numerical and statistical problems", *J. Assoc. Comput. Machinery (ACM)*, **8**(2), 212-229. <https://doi.org/10.1145/321062.321069>
- Jármai K., Snyman J.A., Farkas J. (2006), "Minimum cost design of a welded orthogonally stiffened cylindrical shell", *Comput. Struct.*, **84**(12), 787-797. <https://doi.org/10.1016/j.compstruc.2006.01.002>
- Ji Jin, Ding Xiaohong, Xiong Min (2014), "Optimal stiffener layout of plate/shell structures by bionic growth method", *Comput. Struct.*, **135**(15), 88-99. <https://doi.org/10.1016/j.compstruc.2014.01.022>
- Kaveh A., Kalateh-Ahani M. and Fahimi-Farzam M. (2014), "Life-cycle cost optimization of steel moment-frame structures: performance-based seismic design approach", *Earthq. Struct.*, **7**(3), 271-294. <https://doi.org/10.12989/eas.2014.7.3.271>
- Kaveh A., Fahimi-Farzam M. and Kalateh-Ahani M. (2015), "Optimum design of steel frame structures considering construction cost and seismic damage", *Smart Struct. Syst.*, **16**(1), 1-26. <https://doi.org/10.12989/sss.2015.16.1.001>
- Kim B.J., Y.M. Park, K. Kim and B.H. Choi (2019), "Web bend-buckling strength of plate girders with two longitudinal web stiffeners", *Struct. Eng. Mech.*, **69**(4), 383-397. <https://doi.org/10.12989/sem.2019.69.4.383>
- Kim H.S., Park Y.M., Kim B.J. and Kim K. (2018), "Numerical investigation of buckling strength of longitudinally stiffened web of plate girders subjected to bending", *Struct. Eng. Mech.*, **65**(2), 141-154. <https://doi.org/10.12989/sem.2018.65.2.141>
- Kovács Gy., Farkas J. (2017), "Minimum cost design of overhead crane beam with box section strengthened by CFRP laminates", *Struct. Eng. Mech.*, **61**(4), 475-481. <https://doi.org/10.12989/SEM.2017.61.4.475>
- Mikami I, Niwa K. (1996), "Ultimate compressive strength of orthogonally stiffened steel plates", *J. Struct. Engng ASCE*, **122**(6), 674-682. [https://doi.org/10.1061/\(ASCE\)0733-9445\(1996\)122:6\(674\)](https://doi.org/10.1061/(ASCE)0733-9445(1996)122:6(674))
- Mittelstedt C. (2008), "Explicit analysis and design equations for buckling loads and minimum stiffness requirements of orthotropic and isotropic plates under compressive load braced by longitudinal stiffeners", *Thin-Wall. Struct.*, **46**(12), 1409-1429. <https://doi.org/10.1016/j.tws.2008.03.007>
- Nguyen-Thoi T. et al. (2013), "Static, free vibration and buckling analyses of stiffened plates by CS-FEM-DSG3 using triangular elements", *Comput. Struct.*, **125**, 100-113. <https://doi.org/10.1016/j.compstruc.2013.04.027>

- Paik J.K., Thayamballi A.K., Kim B.J. (2001), "Large deflection orthotropic plate approach to develop ultimate strength formulations for stiffened panels under combined biaxial compression/tension and lateral pressure", *Thin-Wall. Struct.* **39**(3), 215-246. [https://doi.org/10.1016/S0263-8231\(00\)00059-8](https://doi.org/10.1016/S0263-8231(00)00059-8)
- Kim D.K., Poh B.Y., Lee J.R. and Paik J.K. (2018), "Ultimate strength of initially deflected plate under longitudinal compression: Part I = An advanced empirical formulation", *Struct. Eng. Mech.*, **68**(2), 247-259. <https://doi.org/10.12989/sem.2018.68.2.247>
- Recommendations on Fatigue of Welded Components of the International Institute of Welding (2008), Doc. IIW-1823-07, ex. XIII-2151r4-07/XV-1254r4-07.
- Remil A., K.H. Benrahou, K. Draiche, A.A. Bousahla and A. Tounsi (2019), "A simple HSDT for bending, buckling and dynamic behavior of laminated composite plates", *Struct. Eng. Mech.*, **70**(3), 325-337. <https://doi.org/10.12989/sem.2019.70.3.325>
- Rosenbrock H.H. (1960), "An automatic method for finding the greatest or least value of a function", *Comput. J.*, **3**(3), 175-184. <https://doi.org/10.1093/comjnl/3.3.175>
- Simões L.M.C., Farkas J, Jármai K. (2015), "Optimization of a cylindrical shell housing a belt-conveyor bridge", *Comput. Struct.*, **147**(15), 159-164. <https://doi.org/10.1016/j.compstruc.2014.09.015>
- Tran K.L., Douthe C, Sab K, Dallot J, Davaine L. (2014), "Buckling of stiffened curved panels under uniform axial compression", *Construct. Steel Res.*, **103**,140-147. <https://doi.org/10.1016/j.jcsr.2014.07.004>
- Virág Z, Jármai K. (2003), "Parametric studies of uniaxially compressed and laterally loaded stiffened plates for minimum cost", International Conference on Metal Structures (ICMS), Millpress, Rotterdam, 237-242.
- Virág Z. (2006), "Optimum design of stiffened plates", *Pollack Periodica*, **1**(1), 77-92. <https://doi.org/10.1556/Pollack.1.2006.1.6>
- Yoo CH, Choi BH, Ford EM. (2001), "Stiffness requirements for longitudinally stiffened box-girder flanges", *ASCE J. Struct. Eng.*, **127**(6), 705-711. [https://doi.org/10.1061/\(ASCE\)0733-9445\(2001\)127:6\(705\)](https://doi.org/10.1061/(ASCE)0733-9445(2001)127:6(705))
- Žula T, Kravanja S. and Klanšek U. (2016), "MINLP optimization of a composite I beam floor system", *Steel Compos. Struct.*, **22**(5), 1163-1192. <https://doi.org/10.12989/scs.2016.22.5.1163>